Mutagenesis Identifies Amino Acid Residues in Extracellular Loops and within the Barrel Lumen That Determine Voltage Gating of Porin from *Haemophilus influenzae* Type b[†]

Mark A. Arbing,[‡] John W. Hanrahan,[§] and James W. Coulton*,[‡]

Department of Microbiology and Immunology, McGill University, 3775 University Street, Montreal, Quebec, Canada, H3A 2B4, and Department of Physiology, McGill University, 3655 Promenade Sir-William-Osler, Montreal, Quebec, Canada, H3G 1Y6

Received July 26, 2001; Revised Manuscript Received October 5, 2001

ABSTRACT: Porin (341 amino acids; M_r 37 782) of *Haemophilus influenzae* type b mediates exchange of solutes between the external environment and the periplasm of this Gram-negative bacterium. Positively charged residues in the extracellular loops have been shown to be involved in the voltage gating of this protein. To further elucidate our observations on the functional properties of this channel, we mutated seven lysines (Lys^{48}, Lys^{161}, Lys^{165}, Lys^{170}, Lys^{248}, Lys^{250}, and Lys^{253}) to glutamic acid. The selected residues were previously shown to be accessible to chemical modification, and they map to three locations: loop 4 and loop 6, and within the barrel lumen. The seven mutant proteins were purified, and each was reconstituted into planar lipid bilayers to characterize its channel forming properties. The single substitution mutant porins displayed increased single channel conductances in 1 M KCl ranging between 134 and 178% of the single channel conductance for wild-type Hib porin. Six of the seven mutant porins also displayed altered current−voltage relationships when compared to wild-type Hib porin. Whereas Lys^{170}Glu had activity similar to wild-type Hib porin, Lys^{48}Glu, Lys^{248}Glu, and Lys^{253}Glu showed substantial voltage gating at both positive and negative polarities. Lys^{161}Glu and Lys^{250}Glu gated only at negative potentials, and Lys^{165}Glu gated only at positive potentials. Rather than ascribing one specific loop in gating, our analyses of these mutant Hib porins suggest that voltage gating can be attributed to contributions from loops 4 and 6 and a residue within the barrel lumen.

Gram-negative bacteria are protected from the external environment by the selective permeability of the outer membrane (OM).[1] The OM functions to exclude noxious substances in the environment from entering the cell while at the same time allowing the flux of nutrients and metabolic waste products. Most transport across the OM occurs via nonspecific porins, homotrimeric proteins that form water-filled channels and allow the passage of low molecular weight solutes across the OM based on concentration gradients (*1*, *2*). A number of three-dimensional porin structures have been determined by X-ray crystallographic studies (*3*−*8*), and they reveal significant structural homology. Porins form 16-stranded β-barrels with the β-strands connected by long loops on the extracellular surface and by short turns on the periplasmic face of the membrane. One of the long loops (loop 3; L3) folds back into the barrel lumen and is responsible for establishing the molecular mass exclusion limit (*9*). In addition to a molecular mass exclusion limit, porins display other properties including single channel conductance, ion selectivity, and voltage gating (*2*).

Haemophilus influenzae type b (Hib) is a small nonmotile encapsulated bacterium that until recently was the leading cause of bacterial meningitis in developed countries. A protein of approximately 38 kDa in the OM of Hib was found to have pore forming activity and is the unique porin of this bacterial species (*10*). Sequencing of the *ompP2* gene that encodes porin revealed a primary amino acid sequence of 361 amino acids. After cleavage of the signal sequence, a mature peptide of 341 amino acids encodes a protein of 37 782 Da (*11*). Hib porin has a molecular mass exclusion limit of 1400 Da (*10*), a value much higher than that of 600 Da for *E. coli* porins (*12*). Hib may have evolved this property in order to compensate for diminished OM permeability because of having only one major pore forming protein.

Voltage gating of porins has yet to be demonstrated in vivo but may be an effective way to modulate OM permeability. The picture of porins as static sieves has changed with recent evidence demonstrating that porins can be gated in vivo by modulating compounds. Experiments by Delcour and colleagues (*13*) on the *E. coli* porins OmpF and PhoE have shown that the addition of exogenous polyamines inhibited the migration of *E. coli* cells on swarmer plates. Patch clamping experiments (*14*) revealed that polyamines interacted with specific amino acids within the barrel lumen,

[†] This work was supported in part by a grant (MOP-14133 to J.W.C.) from the Canadian Institutes of Health Research.

* To whom correspondence should be addressed at the Department of Microbiology and Immunology, Duff Medical Building, McGill University, 3775 University St., Montreal, QC, H3A 2B4. Tel: 514-398-3929; Fax: 514-398-7052; E-mail: jwcoulton@microimm.mcgill.ca.

[‡] Department of Microbiology and Immunology.

[§] Department of Physiology.

[1] Abbreviations: OM, outer membrane; Hib, *Haemophilus influenzae* type b; nS, nanosiemen(s); SA, succinic anhydride.

10.1021/bi015611y CCC: $20.00
Published on Web 11/03/2001

Table 1: Bacterial Strains and Plasmids Used in This Study

strain or plasmid	relevant characteristics	source, reference
E. coli strains		
DH5α	*supE*44Δ*lac*U169(ϕ80 *lacZ*ΔM15) *hsdR*17 *recA*1 *endA*1 *gyrA*96 *thi-1 relA*1	Life Technologies
XL-1	*recA*1 *endA*1 *gyrA*96 *thi-1 hsdR*17 *supE*44 *relA*1 *lac* [F′ *proAB lacI*^{q}ZΔM15 Tn*10*(Tet^r)]^c	Stratagene
Haemophilus strains		
ATCC9795	wild-type Hib subtype 1H *ompP2*$^+$	(*10*)
DB117	KW20 *rec-1*	(36)
RSFA21	KW20 Δ*ompP2 kan*^{r}	(*24*)
plasmids		
pEJH39-1-35	pGB103 Ω(*Pst*I:: *Eco*RI−*PstI* DL42 2.5-kb *ompP2*$^+$) ColE1 Hi Rep	(*37*)
pFFA02	pBluescript SK(−) Ω(*Pvu*II::*Pvu*II−*Ssp*I pEJH39-1-35 (1-kb sequences coding for mature Hib porin)	(*24*)
pMA01	pEJH39-1-35 (*Mlu*I site in *tet*^{r}eliminated)	
pMUT01 to pMUT07	pFFA02 carrying mutations in mature Hib porin gene	this study
pMA11 to pMA17	pMA01 carrying mutations in mature Hib porin gene	this study

resulting in channel blockage and a concomitant decrease in ion flux through the pore.

Although the structural basis for voltage gating of bacterial porins has not been definitively established, two mechanisms have been postulated. The first mechanism favors movement of the constricting loop, L3, which closes the pore. Mutagenesis experiments (*15*−*17*) that tethered the tip of loop 3 to the barrel wall did not show altered current−voltage relationships compared to wild-type OmpF and PhoE porins. Thus, a more subtle mechanism has been advocated in which rearranged amino acid side chains in the constriction zone close the pore (*18*−*20*). The second proposed mechanism is that the extracellular loops of porin undergo conformational changes in response to applied voltages and thereby occlude the pore. Evidence for this proposal was provided by Muller and Engels (*21*), who observed OmpF using atomic force microscopy. Upon application of voltage, the extracellular loops collapsed into the vestibule of the pore. The authors concluded that this was a mechanism for closing the channel entrance. We also have supporting evidence (*22*) for this mechanism. Substitution of a single arginine residue (Arg^{166}) to a neutral amino acid (Gln) in proposed extracellular loop 4 of Hib porin decreased the critical voltage for gating of Hib porin.

To extend these studies, we chemically modified solvent-accessible lysine residues of Hib porin (*23*). The modification resulted in a heterogeneous population of Hib porins, with 5−11 lysine residues modified per porin. Based on our homology model of Hib porin (*24*), we positioned the modified lysines in the extracellular loops, although one lysine was located in the barrel lumen. The modified Hib porins had a decreased sensitivity to voltage in planar lipid bilayers.

In the present study, we chose to assess the impact of the charges that we had introduced by chemical modification. We made seven single amino acid substitutions of lysine to glutamic acid in three locations: loop 4 (Lys^{161}Glu, Lys^{165}-Glu, Lys^{170}Glu); loop 6 (Lys^{248}Glu, Lys^{250}Glu, Lys^{253}Glu); and within the lumen of the barrel (Lys^{48}Glu). All seven mutants had increased single channel conductance, and six displayed altered current−voltage relationships relative to wild-type Hib porin.

EXPERIMENTAL PROCEDURES

Bacterial Strains, Plasmids, and Media. Strains and plasmids used in this study are listed in Table 1. Nontypeable *H. influenzae* strain DB117 is a recombination-deficient strain derived from Hi parent strain KW20. *Haemophilus* was grown on chocolate agar plates [36 g/L GC base (Difco), 10 g/L hemoglobin (Oxoid), and 20 mL/L IsoVitox supplements (Oxoid)]. Liquid cultures of *Haemophilus* were grown in brain heart infusion (Oxoid) broth supplemented with hemin (10 μg/mL) and NAD^+ (10 μg/mL). Media for *E. coli* strains have been described (*24*). After transformation of *H. influenzae* strains, antibiotic concentrations for selection of chromosomal and plasmid markers were 20 μg/mL kanamycin and 10 μg/mL tetracycline. For selection of plasmid-encoded resistance in *E. coli*, the ampicillin concentration was 100 μg/mL. Antibiotic concentrations were halved in liquid media.

Molecular Biology Techniques. Restriction endonucleases (New England Biolabs) and T4 DNA ligase (Life Technologies) were used in accordance with the manufacturers' recommendations. *E. coli* strain DH5α or Hi strain DB117 were used for isolation of plasmid DNA using plasmid maxi or mini prep kits from QIAGEN. DNA was extracted from agarose gels using a gel purification kit (QIAGEN). *E. coli* cells were made competent for transformation with $CaCl_2$ (*25*); alternatively competent cells were purchased (Stratagene). Hi strains were made competent for DNA uptake using $CaCl_2$ by the method of Barcak et al. (*26*).

Site-Directed Mutagenesis of Hib Porin. Site-directed mutagenesis of Hib porin was performed using the QuikChange site-directed mutagenesis kit (Stratagene) with plasmid pFFA02 as the template. Based on our previous study (*23*), seven lysine residues were selected for mutagenesis; these residues map primarily to surface-exposed residues in our topographical model. Mutagenesis was performed using the primers pLys48Glu, pLys161Glu, pLys165Glu, pLys170Glu, pLys248Glu, pLys250Glu, and pLys253Glu (Table 2) and their reverse complementary oligonucleotides. The mutated regions were sequenced to determine that the desired mutation had been incorporated. Plasmids (pMUT01 to pMUT07) were digested to completion with *Pvu*II and *Mlu*I, and the resulting 1.0 kb *Pvu*II−*Mlu*I DNA fragments containing the mutations were isolated. To facilitate the recombination of the 1.0 kb *Pvu*II−*Mlu*I fragments from plasmids pMUT01 to pMUT07 into Hi vector pEJH39-1-35, a second *Mlu*I restriction site in pEJH39-1-35 was removed using the QuikChange mutagenesis kit the primer pElimlu (Table 2) and its complementary reverse oligonucleotide. The sequence change was confirmed by mapping using

Table 2: Oligonucleotides Used in This Study

oligonucleotide	sequence
pLys48Glu	5′-GGTTCACGTTTCCACATTGAAGCAACT-CATAACTTCGG
pLys161Glu	5′-GCGTGAGGGTGCAGAAGGTGAAAATA-AGCGG
pLys165Glu	5′-GCAAAAGGTGAAAATGAGCGGCCTAA-TGATAAGGC
pLys170Glu	5′-GCGGCCTAATGATGAGGCTGGTGAAGTACG
pLys248Glu	5′-GGCTATGCAAAAACTAAAAACTATGAA-ATTAAACACGAAAAACGCTATTTCG
pLys250Glu	5′-GCAAAAACTAAAAACTATAAAATTGAAC-ACGAAAAACGCTATTTCGTATCTCC
pLys253Glu	5′-CTATAAAATTAAACACGAAGAACGCTATT-TCGTATCTCCAGGTTTCC
pElimlu	5′-CCTCAGCTTCTCAGCGCGTGAAGTGGTTC

restriction enzyme digestion; this plasmid was designated pMA01. The 1.0 kb fragments from pMUT01 to pMUT07 were ligated to the 11.6 kb *Pvu*II−*Mlu*I fragment from pMA01 and used to transform competent Hi host strain DB117; selection was for tetracycline resistance. Recombinant plasmids containing mutations (pMA11 to pMA17) were isolated, sequenced again to confirm the presence of the mutations, and transformed into Hi strain RSFA21; selection was for tetracycline and kanamycin resistances.

Protein Purification. Mutated porins were detergent-extracted from OM preparations as previously described and purified to homogeneity by two-step fast protein liquid chromatography on Q-Sepharose media with Zwittergent Z-3,14 (*27*). The qualities of the protein preparations were assessed by SDS−PAGE followed by staining with Coomassie blue and by silver staining following the protocol of Morrissey et al. (*28*).

Planar Lipid Bilayer Assays. Planar lipid bilayer assays were performed as described previously (*22*, *23*) using a modification of the Mueller and Rudin technique with a bilayer chamber from Warner Instruments. Bilayers were formed from a solution of monoolein at a concentration of 25 mg/mL in *n*-decane, expelling 0.5 μL of lipid solution over a 250 μm aperture. Formation of the bilayer was monitored visually, and the capacitance of the membrane was measured. Once the membrane was stable, protein was added to a final concentration of 1 ng/mL to the cis side of the bilayer chamber using KCl as the electrolyte. Electrical measurements and voltages were applied using an Axopatch 200B amplifier, and data were acquired with the Axoscope software program. Single channel data were organized into histograms, and average single channel conductance was determined by calculating the geometric mean from the histograms. Normal (Gaussian) distribution curves were fit to the histograms with Origin 6.1 software (Microcal, Northampton, MA) to illustrate the changes in conductance values. Using Origin 6.1 software, rate constants (τ) of channel closure were calculated by least-squares fits of single exponentials to macroscopic current decay curves for membranes containing between 25 and 75 channels.

RESULTS

Site-Directed Mutagenesis and Protein Expression of Mutant Hib Porins. To assess the role of charged amino acids in voltage gating of Hib porin, we chose to substitute selected lysine residues with glutamic acid residues. The substitutions

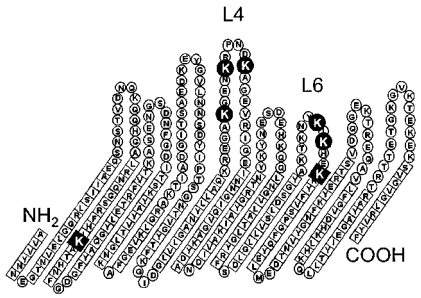

FIGURE 1: Proposed secondary structure diagram of Hib porin. Diagram of the secondary structure of Hib porin based on our tertiary structure model (*24*). Amino acid residues in β-strands are enclosed in diamonds while those amino acids located in turns or loops are enclosed in circles. Lysine residues that have been mutated to glutamic acid are shown in enlarged diamonds (Lys^{48}, Lys^{253}) or in circles [loop 4 (L4): Lys^{161}, Lys^{165}, Lys^{165}; and loop 6 (L6): Lys^{248}, Lys^{250}].

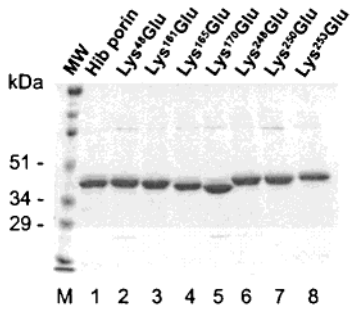

FIGURE 2: Mutant Hib porins purified from *ompP2*-deleted Hi strain RSFA21. Purified protein samples were resolved by SDS−PAGE (10% gel) and stained with Coomassie blue. Lane M, approximately 4 μg of broad-range prestained molecular weight markers (Bio-Rad); lane 1, 3 μg of FPLC-purified wild-type Hib porin; lanes 2−8, 2−4 μg of Hib porins with lysine to glutamic acid mutations.

were made at positions that were targeted by chemical modification in our previous study (*23*) and are proposed to be in three different locations based upon our homology models for secondary and tertiary structure (*24*) of Hib porin: in the barrel lumen, in extracellular loop 4, and in extracellular loop 6 (Figure 1). The constructs were generated with the Stratagene QuikChange site-directed mutagenesis kit, and the fidelity and uniqueness of all mutations were confirmed by DNA sequencing.

Each plasmid harboring the seven different mutations (pMA11 to pMA17) was transformed into Hi strain RSFA21 which is deleted for *ompP2*. From Hi strain RSFA21 OM preparations, the mutant porins were detergent-extracted, purified by anion exchange chromatography, and assessed for their purity and electrophoretic mobility on SDS−PAGE and staining with Coomassie blue (Figure 2). Mutations in loop 4 (Lys^{165}Glu, Lys^{170}Glu; lanes 4, 5) had slightly altered electrophoretic mobilities when compared with the wild-type Hib porin (lane 1). The other mutations (lanes 2, 3, 6, 7, 8) had no effect on electrophoretic mobility.

Single Channel Conductances. Upon reconstitution into planar lipid bilayers, each preparation of purified mutant Hib porin was tested for its channel-forming properties. As all mutant porins formed stable channels, the conductances of approximately 200 channels for each mutant porin were measured. To display the data, conductances are shown as histograms (Figure 3). Each histogram for the seven mutant Hib porins displays a broad distribution of conductance steps

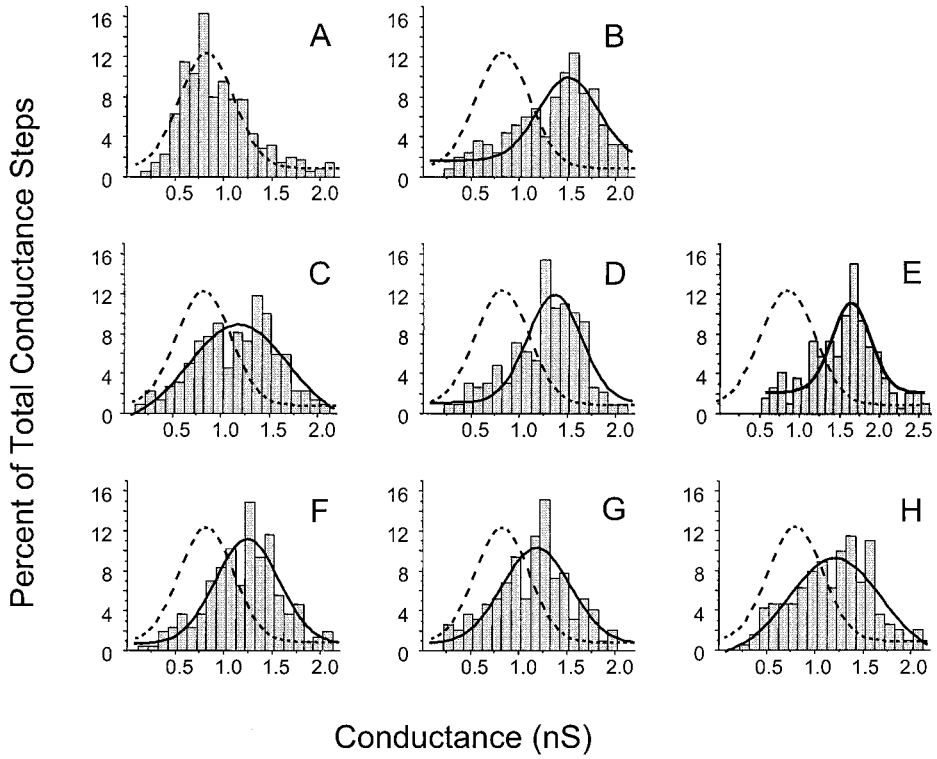

FIGURE 3: Single channel conductances measured in planar lipid bilayers for wild-type Hib porin and the seven mutant Hib porins: wild-type Hib porin (panel A), Lys[48]Glu (panel B), Lys[161]Glu (panel C), Lys[165]Glu (panel D), Lys[170]Glu (panel E), Lys[248]Glu (panel F), Lys[250]-Glu (panel G), Lys[253]Glu (panel H). Mutant Hib porins were diluted with 10 mM Tris, pH 8.0, to 1 ng/μL. Five microliters of this material was added to the cis side of the bilayer chamber containing 1 M KCl so that the final porin concentration was approximately 1 ng/mL. The total number of conductance steps analyzed was as follows: panel A, 249; panel B, 251; panel C, 220; panel D, 227; panel E, 193; panel F, 215; panel G, 192; and panel H, 191. Normal distribution curves were fit to the histograms using MicroCal Origin 6.1. The wild-type Hib porin distribution curve is indicated by a dashed line. This curve has been superimposed on the mutant Hib porin histograms to illustrate the shift in conductance values.

Table 3: Electrophysiological Properties of Hib Porins

				V_c (mV)		τ (s)	
	location	conductance (nS) (SD)	relative conductance (%)	+	−	+80 mV	−80 mV
Hib porin wild type		0.85 (0.44)	100	75	75	103.3 ± 41.6	−
Lys[48]Glu	lumen	1.34 (0.41)	158	30	40	60.3 ± 4.0	90.7 ± 37.9
Lys[161]Glu	loop 4	1.16 (0.36)	136	60	50	N/A	121.3 ± 118.9
Lys[165]Glu	loop 4	1.27 (0.46)	149	40	60	49.8 ± 42.0	N/A
Lys[170]Glu	loop 4	1.51 (0.42)	178	75	75	N/A	N/A
Lys[248]Glu	loop 6	1.16 (0.42)	136	50	40	190.6 ± 69.1	180.0 ± 56.5
Lys[250]Glu	loop 6	1.14 (0.40)	134	−	40	N/A	83.6 ± 4.0
Lys[253]Glu	loop 6	1.19 (0.39)	140	50	50	296.5 ± 33.4	91.5 ± 27.2

with no single conductance increment exceeding 10% of the total conductance steps. When the geometric mean conductance was calculated from the histograms, the mutant Hib porins were found to have significantly increased single channel conductances (Table 3) relative to that reported for wild-type Hib porin (0.85 ± 0.44 nS) in our previous studies (*23*, *24*). In general, mutations in loop 4 produced the largest increases in conductance. The mutants Lys[161]Glu, Lys[165]Glu, and Lys[170]Glu had geometric mean conductances of 1.16 ± 0.41, 1.27 ± 0.36, and 1.51 ± 0.46 nS, respectively, which represent increases of 136%, 149%, and 178% relative to wild-type Hib porin. The mutations Lys[248]Glu, Lys[250]Glu, and Lys[253]Glu in loop 6 had smaller effects on the single channel conductance than the mutations in loop 4. Consistent with mutations in loop 4, these single channel conductance values increased to 136%, 134%, and 140% of the wild-type porin. The geometric mean conductances were 1.16 ± 0.42, 1.14 ± 0.40, and 1.19 ± 0.39 nS for Lys[248]Glu, Lys[250]-Glu, Lys[253]Glu, respectively. Strikingly, mutation of lysine residue Lys[48]Glu within the barrel lumen showed an increase in single channel conductance with a geometric mean conductance of 1.34 ± 0.41, an increase to 158% of wild-type Hib porin single channel conductance. When lower salt concentrations (100 mM KCl) were used, it was found that the relationship between single channel conductance and the bulk aqueous salt concentration for the mutant porins remained linear (data not shown).

Current−Voltage Relationships. Current−voltage relationships for porin molecules are linear (i.e., ohmic) until a critical voltage (V_c) is exceeded. To measure V_c of the mutant Hib porins, we added each mutant to the cis side of the bilayer chamber and waited until porin insertions had stabilized. Most bilayers contained between 25 and 75 porin molecules. To determine the threshold voltage for each porin mutant, the voltage was stepped from a holding potential of 20 mV to higher voltages in increments of 10 mV. Measure-

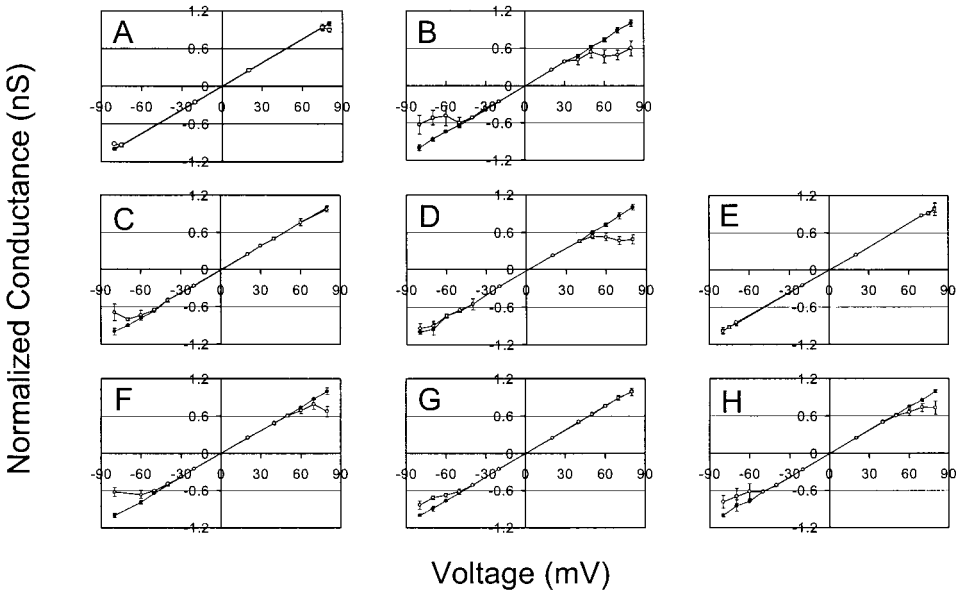

FIGURE 4: Current−voltage curves of planar lipid bilayers containing Hib porin mutants: wild-type Hib porin (panel A), Lys[48]Glu (panel B), Lys[161]Glu (panel C), Lys[165]Glu (panel D), Lys[170]Glu (panel E), Lys[248]Glu (panel F), Lys[250]Glu (panel G), Lys[253]Glu (panel H). Closed circles represent the instantaneous current through membranes while open circles represent steady-state current reached 1−2 min after application of the test voltage. Each symbol represents the values (±SD) from 3−10 experiments. Error bars may lie within the thickness of the symbols. Porin samples were added to the cis side of the chamber after forming bilayers to allow porin insertions from only one side of the chamber.

ments were made at both positive and negative polarities, and the data were normalized and displayed as current−voltage curves with standard deviation (Figure 4). The number of measurements made for each point was between $n = 3$ and $n = 10$. Wild-type Hib porin was found to have a critical voltage of ±75 mV (*22*), and at 80 mV, currents decayed to steady-state levels that were 92% of the instantaneous currents (Figure 4, panel A). The mutant Hib porins had dramatically different current−voltage relationships and reduced V_c (Table 3). The exception was Lys[170]Glu (Figure 4, panel E), which showed similar behavior to wild-type Hib porin. Reversing charge at two other sites in loop 4 reduced V_c and caused the pores to gate at opposite polarity. Lys[165]Glu (Figure 4, panel D) gated at positive potentials with a V_c of 40 mV, a phenotype reminiscent of Hib porin subtypes 2L and 6U (*22*), which have the mutations Arg[166]Asn and Arg[166]Leu, respectively. For the Lys[165]Glu mutation, steady-state currents at +80 mV were 48.3 ± 7.4% of the instantaneous current level. The mutation at Lys[161]Glu (Figure 4, panel C) displayed gating above that of wild-type Hib porin at negative potentials only, with a V_c of −50 mV. The mutant Lys[250]Glu (Figure 4, panel G) had a similar phenotype and gated at negative potentials above a critical voltage of −40 mV, and at positive potentials, it reflected the voltage sensitivity of wild-type Hib porin. Current decay at −80 mV was to 83.2 ± 6.7% of the instantaneous conductance for Lys[250]Glu, while steady-state current levels for Lys[161]Glu were substantially decreased to 69.0 ± 13.3% of the instantaneous current levels.

The remaining mutations in loop 6 [Lys[248]Glu (Figure 4, panel F), Lys[253]Glu (Figure 4, panel H)] had altered phenotypes compared to wild-type Hib porin as both mutant porins gated at both positive and negative polarities. Critical voltages for Lys[248]Glu were −40/+50 mV, and current decay at +80 and at −80 mV was to steady-state levels that were 67.5 ± 8.1% and 61.9 ± 7.1% of instantaneous levels, respectively. Lys[253]Glu critical voltages were ±50 mV, and current decayed at ±80 mV to steady-state levels that were 73.4 ± 10.6% and 78 ± 10.3% of the initial current levels, respectively. Unexpectedly, the Lys[48]Glu mutation showed gating at both polarities. Unlike other mutations in extracellular loops, Lys[48]Glu is situated within the barrel lumen. Previously, only mutations in extracellular loops had been implicated in the voltage gating of Hib porin. Instantaneous currents mediated by Lys[48]Glu decayed to steady-state levels of 60.0 ± 12.0% at +80 mV and 62.9 ± 15.0% at −80 mV. Critical voltages for Lys[48]Glu were +30 and −40 mV.

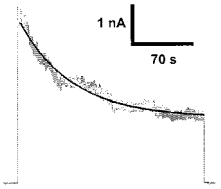

FIGURE 5: Curve fitting to macroscopic current relaxation curves of mutant Hib porin Lys[165]Glu. To determine the rate of entry into the inactivated state, macroscopic current relaxation curves were fit with single exponentials using the least-squares curve-fitting function of the program Origin 6.1 (Microcal). Shown is a representative fit to a macroscopic current relaxation curve of Lys[165]Glu at +80 mV with approximately 60 channels inserted in the bilayer.

Rate of entry into the inactivated state (τ) was determined by fitting a single exponential to the macroscopic current relaxation curve. Most curves were well described by single exponentials (r^2 greater than 0.90). An example of a macroscopic current relaxation curve is displayed in Figure 5. We previously established the rate of closure of Hib porin subtype 1H at +80 mV to be 103.3 ± 41.6 s, a relatively slow process for ion channels. Our succinylated porin (*23*) was found to have a τ of 2.8 ± 0.9 s at + 80 mV. The rate constants for the mutant porins in this study were found to have τ values that were slower or faster than wild-type Hib

porin, but none had values as fast as the succinylated porin (Table 3).

DISCUSSION

This study examines the roles of charged amino acids in determining the electrophysiological properties of Hib porin. Our previous strategy (*23*) was to use chemical modification with succinic anhydride to locate solvent-accessible residues and to test changes in pore-forming properties. We delineated a subset of 11 lysines out of a total of 30 lysine residues in Hib porin that were solvent-accessible and when modified, altered the electrophysiological properties of the pore. The SA-modified Hib porins had lower threshold voltages for gating, and their single channel conductances were increased compared to wild-type Hib porin. By peptide mapping, we identified the modified amino acids within the primary amino acid sequence of Hib porin and their positions within the context of our tertiary structure homology model of Hib porin. Most modified amino acids were predicted to lie in the extracellular loops. In addition, the amino-terminal alanine and a single lysine residue within the barrel lumen (Lys^{48}) were modified. As chemical modification generated a heterogeneous population of Hib porins, it was difficult to assess the impact of charge reversal at the level of single amino acids. In the present study, we chose to make mutations in a defined subset of the SA-targeted lysine residues. Seven lysines were chosen for mutational analysis based on their location within the tertiary structure of our Hib porin homology model. To specifically assess the effect of introducing negative charge at each amino acid position, we made lysine to glutamic acid mutations. The selected residues were Lys^{48}, proposed to be located within the barrel lumen; lysine residues in loop 4 (Lys^{161}, Lys^{165}, Lys^{170}), which we had previously implicated (*22*) in voltage gating of Hib porin; and three lysine residues in loop 6 (Lys^{248}, Lys^{250}, Lys^{253}). We hypothesized that the substitution of some of these lysine residues with glutamic acid would result in altered phenotypes.

Interpretations of the effects of the mutations in this study are based on our homology model for the three-dimensional structure of Hib porin. Our model (*24*) was constructed using a structural scaffold, incorporating data from the atomic resolution structures of three bacterial porins. The model was refined using data from sequence alignments of Hib porin and three other Hi porins. This refinement placed insertions, deletions, and other variable elements within loop and turn regions where the majority of porin sequence variability occurs. The result agrees well with experimental data from our lab and others. First, monoclonal antibodies have been shown in flow cytometry experiments on whole bacterial cells (*29*, *30*) to map to surface-exposed regions defined as loops 4, 5, and 8 in our model. In parallel experiments, antibodies that mapped to loop 3 were found to be nonreactive, thus indicating that loop 3 is not surface-exposed; this is a feature of bacterial porin structures (*3*−*8*). A study of clinical isolates of *H. influenzae* from cystic fibrosis patients also shows that antigenic drift occurs primarily in the regions that we have assigned to loops 1, 2, and 4−8 (*31*). We therefore consider that our three-dimensional model provides an unequivocal framework on which to base predictions about the boundaries of β-strands, loop regions, and turns.

The mutant porins were reconstituted into planar lipid bilayers to assess the effects of the mutations on their functional properties. All mutations showed increases in their single channel conductances relative to wild-type Hib porin. The single channel conductances of the loop 6 mutations (Lys^{248}Glu, Lys^{250}Glu, and Lys^{253}Glu) were increased to 130−140% relative to the wild-type protein. Single channel conductances of the loop 4 mutations (Lys^{161}Glu, Lys^{165}Glu, and Lys^{170}Glu) were increased, but to levels that were 140−170% of the wild-type Hib porin conductance. We attribute this to the role of the extracellular loops in narrowing the entrance, or vestibule, of the pore. In our homology model (*24*), loop 4 has a length of 23 amino acids, and loop 6 has a length of 11 amino acids. The crystal structure of OmpF porin (*4*) shows that several of the extracellular loops, including loops 4 and 6, are inclined toward the central axis of the pore. Consistent with this, deleting 6 or 12 amino acids from loop 4 increased the single channel conductance to 135% or 124% of wild-type Hib porin, respectively (*24*). The results suggest that loop 4 is oriented toward the central pore in Hib porin, as in OmpF, and that such deletions increase conductance by widening the pore entrance. In the present study, we show that targeted mutations in the extracellular loops increase single channel conductance in a similar manner. Introduction of negative charge into the loops is suggested to alter electrostatic interactions and reorient the loops, resulting in an enlargement of the pore entrance. Thus, the pore would become more accessible to the ions in solution, and single channel conductance would increase. This is consistent with our previous study using chemical modification (*23*) in which the single channel conductance of SA-modified porin was increased relative to wild-type Hib porin (1.24 ± 0.41 versus 0.85 ± 0.40 nS, respectively).

The mutation in the constriction zone of the barrel increased single channel conductance to 158% (1.34 ± 0.41 nS) of the wild-type conductance. We propose two possible explanations for this increase in conductance. The introduction of a new negative charge into the barrel lumen may result in a repositioning of loop 3 and an increased pore size, thus increasing single channel conductance. Alternatively, the addition of the extra negative charge may result in a pore that is more efficient at cation conduction, thereby enhancing the transport properties of this cation-selective pore. Schmid and colleagues (*32*) altered the charge pattern of the cation-selective porin of *Rhodopseudomonas blastica* and found that the removal of positive charges increased conductance while removing negative charges decreased conductance. However, the changes in conductance were small; therefore, it was concluded that ion permeation did not critically depend on those charges near the constriction site. Decreasing the size of the constriction zone by introducing up to six tryptophans had a significantly greater effect as the single channel conductances were noticeably reduced as compared to wild-type porin. Additional studies by Saxena et al. (*33*) with the weakly anion-selective porin of *Paracoccus denitrificans* found that removal of single positive charges that are involved in attracting anions effectively reduced the conductance. However, the authors noted that channel behavior was more difficult to predict when multiple charges were removed, specifically those that determine porin selectivity. A recent study by Phale et al. (*20*) also found that removal of charge from the constriction zone of OmpF reduced single

channel conductivities. Some of the mutants resulted in increased pore size at the constriction zone, and the authors concluded that pore size and amino acid charge within the constriction zone are both responsible for conductivity levels.

In the present study, mutant Hib porins were reconstituted into planar lipid bilayers, and their voltage gating properties were characterized. A variety of different phenotypes were found with the mutant Hib porins including a phenotype identical to Hib porin subtype 1H, others that were similar to Hib porin subtypes 2L and 6U (*22*), as well as novel phenotypes. The substitution at Lys^{170} in loop 4 showed similar properties as wild-type Hib porin 1H; the pore was essentially voltage-independent as this residue may not be in a position to interact with other charged residues in the extracellular loops. The mutation $Lys^{165}Glu$ displayed current−voltage relationships similar to those of Hib porin subtypes 2L and 6U (*22*). The porin gated only at positive potentials with a similar critical voltage and extent of current decay. Such loss of positive charge in consecutive amino acid residues gives a similar phenotype, suggesting that pore closure results from a similar action of loop 4 in both porin variants. A third substitution in loop 4, $Lys^{161}Glu$, was responsive to voltages of negative polarity only. The extent of current decay was less than that seen for mutation Lys^{165} at positive polarity. Thus, the position of the mutation is clearly important in determining both the sensitivity of the porin to voltage as well as the extent of current decay.

All mutant porins with changes in loop 6 showed altered voltage gating. The mutations $Lys^{248}Glu$ and $Lys^{253}Glu$ showed similar current−voltage relationships, with gating at both positive and negative polarity. The critical voltages for these mutants were similar, and the extent of closure was also comparable. In contrast, the mutation $Lys^{250}Glu$ gated only at negative polarity. The extent of current decay for $Lys^{250}Glu$ was similar to $Lys^{253}Glu$, and their critical voltages were the same. In our tertiary structure model, Lys^{253} is located at the top of β-strand 13 while the other two mutations are found closer to the apex of loop 6. It is difficult to attribute the differences in voltage gating activity of these mutants to location of charged residue because the mutations are close to each other. Nevertheless, our data show unequivocally that introduction of negative charge into loop 6 increases voltage sensitivity. Loop 6, in addition to loop 4, can now be implicated in the voltage gating of Hib porin.

The values of τ were determined for the mutant porins at voltages of ± 80 mV, where the pore showed substantial voltage-dependent gating. We showed previously (*23*) that entry of wild-type Hib porin into the inactivated state is slow at $+80$ mV whereas our SA-modified porin entered the inactivated state rapidly (2.8 ± 0.9 s). In this study, we measured the rate constants and found that the mutants $Lys^{165}Glu$ (loop 4), $Lys^{250}Glu$ (loop 6), and $Lys^{48}Glu$ (barrel lumen) had closing rates that were fast compared to wild-type Hib porin. When τ was determined for the remaining mutations in loop 4 ($Lys^{161}Glu$) and loop 6 ($Lys^{248}Glu$, $Lys^{253}Glu$), it was found that they generally entered the inactivated state more slowly than wild-type Hib porin. None of the mutant porins entered into the inactivated state as rapidly as the SA-modified porin from our previous study. Clearly the rate of entry into the inactivated state becomes faster with the introduction of multiple negative charges (SA-modified porin).

Consistent with our hypothesis that voltage gating of Hib porin is due to conformational changes in extracellular loops, six mutations in this study were located in extracellular loops, and five showed altered phenotypes. These mutations provide further support for our hypothesis that voltage gating of Hib porin is due to conformational changes in the extracellular loops. On the other hand, the most striking phenotype was that of $Lys^{48}Glu$, located in β-strand 3 in our homology model. Reports by Schmid et al. (*32*), Saint et al. (*19*), and Phale et al. (*20*) have shown that altering the charge at the pore constriction results in pores that are either more or less sensitive to external voltages than the wild-type pore. Our results show that voltage gating of Hib porin can also result from changes in the charge pattern within the constriction zone. Our data further demonstrate differences in voltage gating upon modifying the charge in the pore lumen, illustrating the similarity of Hib porin to other bacterial porins.

We now propose that voltage gating of Hib porin can occur through two possible mechanisms. The first postulates that charged residues in the extracellular loops may allow for conformational changes to occur under applied potentials. These conformational changes would result in an occlusion of the pore entrance and thereby reduce current through the pore. Support for this comes from our work on Hib porins that have altered charge in the extracellular loops and from the observations of Muller and Engels (*21*), who used atomic force microscopy to visualize conformational changes in the extracellular loops of OmpF in response to voltage. This mechanism is also consistent with studies of other β-barrel proteins such as *S. aureus* α-hemolysin, which exhibits voltage gating but lacks a constriction loop that could block the pore (*34*, *35*). The second mechanism we propose for voltage gating of Hib porin is that structural changes occur within the constriction zone of the β-barrel. Considerable evidence for this mechanism comes from studies on voltage gating of *E. coli* OmpF and PhoE porins (*18*−*20*) and the porins of *R. capsulatus* (*32*) and *P. denitrificans* (*33*), but the structural basis remains unclear. Moreover, a recent study on *E. coli* OmpF (*20*) showed no dependence of voltage gating on charge substitution in the pore lumen.

We conclude that two modes of pore closure may result from the application of transmembrane voltages. Mutations that we made in the extracellular loops are distant from the constriction zone, and yet they affect voltage gating, supporting a mechanism in which the extracellular loops are responsible for pore closure. However, the mutation of Lys^{48} to glutamic acid and its subsequent lower threshold for voltage gating favor the alternate hypothesis: that voltage gating of porins is a feature due to the unique geometry of the constriction zone and the transverse electric field at this location. That amino acid residues from the two locations may interact during gating cannot be discounted, nor can the possibility that changes in protein conformation in one part of the porin might promote conformational changes in another location. A high resolution structure for Hib porin would allow us to identify residues in the extracellular loops that interact with critical L4 and L6 residues, but an approach that monitors conformational changes will be required for a fully integrated model of voltage gating.

ACKNOWLEDGMENT

DNA sequencing and oligonucleotide synthesis were performed by the Sheldon Biotechnology Center, McGill University. We appreciate critical reviews of the manuscript by C. M. Khursigara and P. Pawelek, and the editorial support of J. A. Kashul.

REFERENCES

1. Koebnik, R., Locher, K. P., and Van Gelder, P. (2000) *Mol. Microbiol. 37*, 239−253.
2. Schirmer, T. (1998) *J. Struct. Biol. 121*, 101−109.
3. Weiss, M. S., Kreusch, A., Schiltz, E., Nestel, U., Welte, W., Weckesser, J., and Schulz, G. E. (1991) *FEBS Lett. 280*, 379−382.
4. Cowan, S. W., Schirmer, T., Rummel, G., Steiert, M., Ghosh, R., Pauptit, R. A., Jansonius, J. N., and Rosenbusch, J. P. (1992) *Nature 358*, 727−733.
5. Kreusch, A., Neubuser, A., Schiltz, E., Weckesser, J., and Schulz, G. E. (1994) *Protein Sci. 3*, 58−63.
6. Hirsch, A., Breed, J., Saxena, K., Richter, O. M., Ludwig, B., Diederichs, K., and Welte, W. (1997) *FEBS Lett. 404*, 208−210.
7. Dutzler, R., Rummel, G., Alberti, S., Hernandez-Alles, S., Phale, P., Rosenbusch, J., Benedi, V., and Schirmer T. (1999) *Struct. Fold. Des. 7*, 425−434.
8. Zeth, K., Diederichs, K., Welte, W., and Engelhardt, H. (2000) *Struct. Fold. Des. 8*, 981−992.
9. Jap, B. K., and Walian, J. P. (1996) *Physiol. Rev. 76*, 1073−1088.
10. Vachon, V., Lyew, D., and Coulton, J. W. (1985) *J. Bacteriol. 162*, 918−924.
11. Munson, R. S., Jr., and Tolan, R. W., Jr. (1989) *Infect. Immun. 57*, 88−94.
12. Nikaido, H. (1992) *Mol. Microbiol. 6*, 435−442.
13. delaVega, A. L., and Delcour, A. H. (1995) *EMBO J. 304*, 216−220.
14. Iyer, R., and Delcour, A. H. (1997) *J. Biol. Chem. 272*, 18595−18601.
15. Bainbridge, G., Mobasheri, H., Armstrong, G. A., Lea, E. J. A., and Lakey, J. H. (1998) *J. Mol. Biol. 275*, 171−176.
16. Phale, P. S., Schirmer, T., Prilipov, A., Lou, K.-L., Hardmeyer, A., and Rosenbusch, J. P. (1997) *Proc. Natl. Acad. Sci. U.S.A. 94*, 6741−6745.
17. Eppens, E. F., Saint, N., Van Gelder, P., van Boxtel, R., and Tommassen, J. (1997) *FEBS Lett. 415*, 317−320.
18. Van Gelder, P., Saint, N., Phale, P., Eppens, E. F., Prilipov, A., van Boxtel, R., Rosenbusch, J. P., and Tommassen, J. (1997) *J. Mol. Biol. 269*, 468−472.
19. Saint, N., Lou, K.-L., Widmer, C., Luckey, M., Schirmer, T., and Rosenbusch, J. P. (1996) *J. Biol. Chem. 271*, 20676−20680.
20. Phale, P. S., Philippsen, P., Widmer, C., Phale, V. P., Rosenbusch, J. P., and Schirmer, T. (2001) *Biochemistry 40*, 6319−6325.
21. Müller, D. J., and Engel, A. (1999) *J. Mol. Biol. 285*, 1347−1351.
22. Dahan, D., Vachon, V., Laprade, R., and Coulton, J. W. (1994) *Biochim. Biophys. Acta 1189*, 204−211.
23. Arbing, M. A., Dahan, D., Boismenu, D., Mamer, O. A., Hanrahan, J. W., and Coulton, J. W. (2000) *J. Membr. Biol. 178*, 185−193.
24. Srikumar, R., Dahan, D., Arhin, F. F., Tawa, P., Diederichs, K., and Coulton, J. W. (1997) *J. Biol. Chem. 272*, 13614−13621.
25. Sambrook, J., Fritsch, E. F., and Maniatis, T. (1989) *Molecular Cloning: A Laboratory Manual*, Cold Spring Laboratory, Cold Spring Harbor, NY.
26. Barcak, G. J., Chandler, M. S., Redfield, R. J., and Tomb, J.-F. (1991) *Methods Enzymol. 204*, 321−342.
27. Srikumar, R., Chin, A. C., Vachon, V., Richardson, C. D., Ratcliffe, M. J. H., Saarinen, L., Käyhty, H., Mäkelä, P. H., and Coulton, J. W. (1992) *Mol. Microbiol. 6*, 665−676.
28. Morrissey, J. H. (1981) *Anal. Biochem. 117*, 307−310.
29. Srikumar, R., Dahan, D., Gras, M. F., Ratcliffe, M. J. H., van Alphen, L., and Coulton, J. W. (1992) *J. Bacteriol. 174*, 4007−4016.
30. Haase, E. M., Yi, K., Morse, G. D., and Murphy, T. F. (1994) *Infect. Immun. 62*, 3712−3722.
31. Regelink, A. G., Dahan, D., Möller, L. V. M., Coulton, J. W., Eijk, P., van Ulsen, P., Dankert, J., and van Alphen, L. (1999) *Antimicrob. Agents Chemother. 43*, 226−232.
32. Schmid, B., Maveyraud, L., Krömer, M., and Schulz, G. E. (1998) *Protein Sci. 7*, 1603−1611.
33. Saxena, K., Drosou, V., Maier, E., Benz, R., and Ludwig, B. (1999) *Biochemistry 38*, 2206−2212.
34. Song, L., Hobaugh, M. R., Shustak, C., Cheley, S., Bayley, H., and Gouaux, J. E. (1996) *Science 274*, 1859−1866.
35. Korchev, Y. E., Alder, G. M., Bakhramov, A., Bashford, C. L., Joomun, B. S., Sviderskaya, E. V., Usherwood, P. N., and Pasternak, C. A. (1995) *J. Membr. Biol. 143*, 143−151.
36. Setlow, J. K., Boling, M. E., Beattie, K. L., and Kimball, R. F. (1972) *J. Mol. Biol. 68*, 361−378.
37. Cope, L. D., Pelzel, S. E., Latimer, J. L., and Hansen, E. J. (1990) *Infect. Immun. 58*, 3312−3318.

BI015611Y